American Mineralogist, Volume 88, pages 1428–1435, 2003

Pressure-controlled polytypism in hydrous layered materials

PRZEMYSLAW DERA,[1,*] CHARLES T. PREWITT,[1] STEFANIE JAPEL,[1,2] DAVID L. BISH,[3] AND CLIFF T. JOHNSTON[4]

[1]Geophysical Laboratory, Carnegie Institution of Washington, 5251 Broad Branch Road, NW, Washington, D.C. 20015, U.S.A.
[2]Department of Earth and Planetary Sciences, Johns Hopkins University, Olin Hall, 3400 North Charles Street, Baltimore, Maryland 21218, U.S.A.
[3]Geology and Geochemistry, MS D469, Los Alamos National Laboratory, Los Alamos, New Mexico 87545, U.S.A.
[4]Birck Nanotechnology Center, 915 W. State Street, Purdue University, West Lafayette, Indiana 47907-2054, U.S.A.

ABSTRACT

An isosymmetric displacive structural transformation in the hydrous layer silicate dickite [$Al_2Si_2O_5(OH)_4$, monoclinic *Cc*, $a = 5.161(3)$, $b = 8.960(6)$, $c = 14.459(10)$ Å, $\beta = 96.77(1)°$], occurring under hydrostatic compression above 2.0 GPa, has been studied using single-crystal X-ray diffraction and diamond-anvil cell techniques. The structure of the high-pressure phase, determined in situ, is monoclinic with space group *Cc* with unit-cell parameters $a = 5.082(3)$, $b = 8.757(6)$, $c = 13.771(9)$ Å, and $\beta = 89.60(2)°$ at 4.1 GPa. The positions of all hydrogen atoms at both ambient and high pressure have been determined by a combination of simulated annealing and energy minimization. The mechanism of the transformation, which may be general for other hydrous layered materials, involves a shift of the 1:1 layers with respect to each other by the vector [1/6, 1/6, 0] and is accompanied by the formation of new hydrogen bonds.

INTRODUCTION

Polytypism is a particular type of polymorphism, occurring only in layered structures, in which the different polytypes share the same, common structure of the individual layer, whereas the layer-stacking scheme is different (Verma and Krishna 1966). In many respects inter-polytype transformations may be considered as a direct analogy of Rigid Unit Mode (RUM) transformations in framework structures (Dove et al. 2000), with the exception that in layered structures the whole layers play the role of rigid units. The most common natural materials exhibiting polytypism include phyllosilicates and layered hydroxides. These materials show high anisotropy, resulting from interlayer forces that are much weaker than the intralayer forces. The interlayer forces in layered materials include electrostatic and van der Waals interactions, and, depending on the composition of the material, as well as the presence of interlayer species (metal ions, water molecules, small organic molecules, etc.), may also include hydrogen bonding (see, e.g., Giese 1973). The small energy differences between different polytypes, as well as the anisotropy of the interatomic forces often cause polytypism to manifest itself in the form of stacking fault formation rather than formation of separate phases. The subtle balance between the different kinds of interlayer forces controlling which polytype is energetically favorable can be significantly affected by external stimuli, including a change in temperature or pressure. Of these two thermodynamic parameters, pressure is a much more powerful controlling factor, driving transformations toward structures with higher density and smaller volume. Because of the small energy changes involved, pressure-driven inter-polytype transformations should generally occur at relatively low pressure (<5 GPa), which is easily accessible in a high-pressure diamond-anvil cell. The high-pressure behavior of layered structures remains relatively unexplored, however, primarily due to the lack of good quality single-crystal specimens.

There have been several previous attempts to characterize the high-pressure behavior of various phyllosilicates. Holtz et al. (1993) studied talc, biotite, phlogopite, margarite, and muscovite at high pressures using Raman spectroscopy. On the basis of the observed changes in the spectra they concluded that these minerals undergo fairly complex deformation, but no discontinuous changes in pressure dependencies of Raman mode frequencies were observed. The effects of pressure on di- and trioctahedral micas have been studied by several groups. Catti et al. (1994), Faust and Knittle (1994), and Comodi and Zanazzi (1995) studied compression of muscovite and concluded that, apart from amorphization occurring above 20 GPa, compression proceeds continuously with no structural phase transitions. Similarly, no phase transitions were found in paragonite up to 4 GPa (Comodi and Zanazzi 1997) or in phlogopite and chlorite (Hazen and Finger 1978). Among layered hydroxides only brucite [$Mg(OH)_2$] and gibbsite [$Al(OH)_3$] have been studied systematically (Duffy et al. 1995; Huang et al. 1996; Huang et al. 1999; Parise et al. 1994; Catti et al. 1995). In both examples structural phase transitions involving rearrangements of hydrogen bonds occur at relatively moderate pressures (<5 GPa).

A very interesting group of hydrous layered-materials is the family of 1:1 dioctahedral phyllosilicates known as the kaolin minerals. The kaolin minerals, kaolinite, dickite, and nacrite, with composition $Al_2Si_2O_5(OH)_4$, as well as halloysite, the hy-

* E-mail: pdera@gl.ciw.edu

drated species, are among the most common clay mineral groups on the surface of the Earth (Murray 1991). The 1:1 layers in kaolin minerals are weakly bonded to one another, primarily via hydrogen bonds. These minerals can be regarded as model systems for inorganic hydrous phases where hydrogen bonds compete with other interatomic interactions, influencing crystal packing and energetics (Giese 1991).

The transformations that clay minerals undergo when exposed to high temperatures and pressures are of great interest for both fundamental and applied science. Kaolins occur in nature in a variety of environments, and hydrothermal influences on their structures and properties are important for understanding their genesis and geological transformations. We know from surface exposures that fault gouge of various compositions occurs along active tectonic faults (e.g., the San Andreas Fault). There is a discrepancy between the shear stress required to initiate rock-on-rock sliding and the shear stress on the San Andreas fault and other active tectonic areas (Zoback and Roller 1979). Early laboratory studies (Velde 1969) showed that kaolinite and montmorillonite form a stable mineral assemblage at pressures up to 3.5 GPa and temperatures below 420 °C. Wang et al. (1978) suggested that clay minerals can be present in large quantities at midcrustal depths along active faults, and their presence has been used to explain these discrepancies. Therefore, knowledge of the mechanical and elastic properties of clays is important to understand and explain the behavior of faults (Wang et al. 1979, 1980). Despite the importance of the problem, no systematic structural studies of the effects of pressure on 1:1 phyllosilicates were available prior to our study, except for nonhydrostatic mechanical deformation (Wang et al. 1979, 1980) and grinding experiments (LaIglesia 1993).

Recently, Johnston et al. (2002) presented results of a single-crystal Raman study of dickite at pressures up to 6.5 GPa using a diamond-anvil cell. They found a dramatic shift in the ν(OH) bands at ~2.2 GPa, indicating a significant change in the local environment of the interlayer OH groups. The lattice mode region showed only minor changes as a function of pressure, suggesting that the individual 1:1 layers did not change significantly with pressure. The spectra also showed that the phase transition is reversible. The aim of the current study is to evaluate the structural basis of this phase transition by in situ high-pressure single-crystal X-ray diffraction.

EXPERIMENTAL METHODS

A single crystal of dickite, approximately $0.2 \times 0.2 \times 0.1$ mm in size, from the St. Claire, Pennsylvania locality, was obtained from Wards Natural Science Establishment, Inc, and was mounted in a Merrill-Bassett diamond anvil cell (DAC) equipped with beryllium discs. The sample was attached to the surface of one of the diamond anvils with a smear of vaseline. A methanol-ethanol mixture was used as a hydrostatic pressure medium. Three ruby chips were placed inside the DAC for pressure calibration, together with the sample crystal. Full single-crystal X-ray diffraction (XRD) data sets were collected at 0.1 MPa, before mounting the sample in the DAC, and at 4.1 GPa, during compression. Additional limited sets of data at 1.9 and 2.5 GPa were collected for unit-cell parameter determination.

All X-ray experiments were carried out with an automated Bruker AXS *P*4 diffractometer equipped with a SMART 1K CCD detector. The instrument employed graphite-monochromated Mo$K\alpha$ radiation. The incident beam was collimated to a diameter of 0.3 mm. The sample-to-detector working distance was approximately 70 mm. High-pressure experiments with the DAC were performed in series of eight scans at $\chi = 0$, 30, 60, and 90°, and $\varphi = 0$ and 180°. An exposure time of 30 s was employed for all DAC experiments. Much shorter experiments with two scans at $\chi = 0°$ and $\chi = 90°$ and $\varphi = 0°$ were performed for evaluation of changes in unit-cell parameters.

The data were corrected for geometrical distortion, dark current, and flood-field effects. Sample crystal orientation for ambient pressure experiments was determined using the Bruker SMART program. High-pressure experiments used a suite of programs written in our lab. Integrated intensities were calculated using the Bruker SAINT program and were corrected for Lorentz and polarization effects. An absorption correction was applied using the SADABS program, and an empirical correction program written in our lab was used to account for absorption by the components of the high-pressure cell for DAC data.

The structure of dickite above the transition pressure was solved using direct methods and the SIR97 (Giacovazzo 1997) program. Refinement was performed using SHELXL from the SHELXTL package (Sheldrick 1997). The details of the structure refinements and the fractional atomic coordinates from the refinement are given in Tables 1 and 2. Anisotropic displacement parameters (ADPs) were used for all non-hydrogen atoms in the ambient-pressure refinement. For the high-pressure data set, because of the lower quality of intensity data and smaller number of observations, isotropic displacement parameters (IDP) were applied. Additionally, to reduce the number of independent variables being refined, the IDPs were constrained to be equal for the same type of ions at high pressure. Initial hydrogen atom positions were taken from the Endeavour program. The Endeavour program applies Lennard-Jones interatomic potentials parameterized to reproduce the expected interatomic distances (determined on the basis of crystal chemistry), estimates the total energy of each tested structure model to avoid unreasonable structures (unreasonably short interatomic contacts), and to evaluate appropriateness of the model from an energetic point of view. The statistical weight of the contribution from *R*-factor and repulsion energy to the figure of merit in the structure optimization algorithm is determined by a cost function.

At ambient pressure the H atom coordinates were refined with soft restraints imposed on the O-H distance (distance required to be close to 0.9 Å). For high-pressure data H atom coordinates obtained from Endeavour were fixed and excluded from the refinement. IDPs for hydrogen atoms were not refined, but fixed at 120% of the value of isotropic equivalents of ADP for the O atom to which the H atom was connected.

RESULTS AND DISCUSSION

The phase transition was observed to occur between 1.9 and 2.5 GPa, in agreement with the Raman results of Johnston et al. (2002). The space group of high-pressure dickite is the same as that of the low-pressure form, as are the Wyckoff positions of all the atoms. Therefore, the transformation can be classified as "type-0" isosymmetric according to the classification introduced by Christy (1993, 1995). As expected for a type-0 phase transition, the high-pressure transformation in dickite is of first order, accompanied by a small discontinuous decrease in unit-cell volume. The primary difference between the two structures is a reduction of the β angle from 96.7° in dickite at 1.9 GPa to 89.6° in high-dickite at 4.1 GPa. The topology of the individual 1:1 layers, as well as their orientation remained unchanged after the transformation, whereas the stacking scheme and the interlayer hydrogen bonding topology changed significantly.

Interlayer bonding in kaolin minerals

The absence of cations in the interlayer regions of kaolin minerals makes the role of interlayer hydrogen bonds very significant. Many previous authors, including Newnham (1961), Zvyagin (1962), and Brindley and Brown (1980), analyzed the possible polytypic varieties in the kaolin group. However, to better understand the topological relationships between the low- and high-pressure polytypes of dickite, a slightly different approach can be applied: in our considerations we will concen-

TABLE 1. Crystal data and structure refinements for low- and high-pressure dickite

Pressure	0.1 MPa	4.1 GPa
Crystal system, space group	monoclinic, *Cc*	monoclinic, C*c*
Unit cell dimensions	*a* = 5.161(3) Å	*a* = 5.082(3) Å
	b = 8.960(6) Å	*b* = 8.757(6) Å
	c = 14.46(1) Å	*c* = 13.77(1) Å
	β = 96.77(1)°	β = 89.60(2)°
Volume	663.9(7) Å^3	612.9(7) Å^3
Z, Calculated density	2, 2.583 g/cm^3	2, 2.798 g/cm^3
Wavelength	0.71073 Å	0.71073 Å
Θ range	4.55 to 25.51°	4.64 to 22.21°
Limiting indices	$-3 \le h \le 6$, $-8 \le k \le 10$, $-15 \le l \le 17$	$-5 \le h \le 1$, $-9 \le k \le 7$, $-5 \le l \le 4$
Refl. collected/unique	1455 / 793 (R_{int} = 0.0987)	569 / 198 (R_{int} = 0.1559)
Data/restraints/parameters	793 / 6 / 131	198 / 32 / 55
Goodness-of-fit on F^2	0.962	1.003
Final *R* indices [$I > 2\sigma(I)$]	R_1 = 0.0521, wR_2 = 0.0795	R_1 = 0.0650, wR_2 = 0.1146
R indices (all data)	R_1 = 0.0804, wR_2 = 0.0884	R_1 = 0.1447, wR_2 = 0.1424
Extinction coefficient	0.007(1)	0.027(6)
Largest diff. peak and hole	0.574 and –0.522 e Å^{-3}	0.347 and –0.457 e Å^{-3}

TABLE 2. Atomic coordinates and equivalent isotropic displacement parameters (Å$^2 \times 10^3$) for low- and high-pressure dickite refined from the X-ray data

Atom	*x*	*y*	*z*	U_{eq}
	Low pressure dickite at 0.1 MPa			
Si1	0.0088(5)	0.4010(3)	0.0324(2)	12(1)
Si2	–0.0035(5)	0.0722(3)	0.0315(2)	10(1)
Al1	0.9126(5)	0.2523(3)	0.2233(2)	16(1)
Al2	0.4184(7)	0.4176(4)	0.2226(3)	18(1)
O1	0.956(1)	0.2380(8)	0.9864(4)	17(2)
O2	0.255(1)	0.4714(7)	0.9856(5)	18(2)
O3	0.764(1)	0.5058(8)	0.9991(5)	17(2)
O4	0.079(2)	0.3908(8)	0.1428(7)	21(2)
O5	0.003(1)	0.0807(8)	0.1443(6)	12(2)
OH1	0.585(1)	0.2747(9)	0.1488(5)	22(2)
OH2	0.243(2)	0.278(1)	0.2866(7)	18(2)
OH3	0.253(2)	0.893(1)	0.2888(7)	15(2)
OH4	0.323(2)	0.584(1)	0.2863(8)	21(3)
H1	0.57(2)	0.173(3)	0.152(8)	26
H2	0.31(2)	0.26(1)	0.346(3)	22
H3	0.25(2)	0.990(4)	0.305(7)	18
H4	0.27(2)	0.59(1)	0.342(4)	26
	High pressure dickite at 4.1 GPa			
Si1	0.046(2)	0.488(1)	0.038(2)	5(2)
Si2	0.033(2)	0.159(1)	0.037(2)	5(2)
Al1	0.879(2)	0.335(2)	0.233(2)	5(2)
Al2	0.386(2)	0.500(1)	0.234(2)	5(2)
O1	0.987(3)	0.324(3)	0.986(4)	0(6)
O2	0.316(4)	0.550(2)	–0.009(4)	4(4)
O3	0.827(4)	0.606(3)	–0.004(4)	7(4)
O4	0.071(4)	0.478(3)	0.155(5)	8(4)
O5	0.002(3)	0.170(3)	0.155(4)	6(4)
OH1	0.578(3)	0.360(3)	0.161(5)	3(4)
OH2	0.197(3)	0.353(2)	0.304(4)	5(4)
OH3	0.190(5)	0.984(3)	0.303(5)	10(5)
OH4	0.262(5)	0.666(3)	0.301(5)	11(4)
H1	0.4964	0.2556	0.1421	
H2	0.2349	0.2821	0.3511	
H3	0.2518	0.0170	0.3557	
H4	0.2329	0.6345	0.3701	

Note: U_{eq} is defined as one third of the trace of the orthogonalized U_{ij} tensor.

trate on the interlayer region, and therefore we will describe the stacking types focusing only on the Si and Al sheets connected by hydrogen bonds, belonging to neighboring 1:1 layers. In such an approach the rotation of the neighboring 1:1 layers is ignored. There are two distinct ways the Al and Si sheets in the interlayer region may be stacked over one another, as illustrated in Figure 1. To optimize interlayer hydrogen bonding, they may be:

Type I: shifted with respect to one another by the $[-2/3, -1/3]_h$* vector of the hexagonal 2-D lattice, or $[-1/2, -1/6]_r$ of the rectangular 2-D lattice, as in kaolinite and dickite, with the amplitude of the layer shift about 3.0 Å†. In this case, half of the Si ions within one layer overlap Al ions in the next layer, and the other half is placed above the voids in the Al sheet of the next layer.

Type II: shifted with respect to one another by the $[-1/3, 0]_h$ or $[-1/3, 0]_r$ vector, as in nacrite, with the amplitude of the layer shift about 1.7 Å‡ In this case all the Si atoms have two equidistant nearest neighbors in the Al sheet of the next layer.

In such a simplified approach, kaolinite and dickite have the same layer stacking, Type I, whereas nacrite represents Type II stacking. Both types of layer stacking optimize formation of interlayer O-H···O hydrogen bonds. For the two examples of Type-I and Type-II stacking described above, to convert the former into the latter, a shift of layers by the vector $[1/6, 1/6]_r$ ($[1/3, 1/3]_h$), or its equivalent is necessary, which corresponds to a translation amplitude of about 1.7 Å. In the monoclinic unit cell of dickite, the layers are approximately normal to the **c***-direction. The layer shift in dickite is allowed by the *Cc* space group and is reflected by an average shift of all the atoms in the unit cell by the $[-0.014, 0.077]_r$ vector. The (010) *c*-glide plane is perpendicular to the layers and the neighboring layers are related to each other by this symmetry operation, therefore a change in fractional atomic coordinate *y* results in the relative interlayer shift 2*y*. As a result, the effective layer shift along **b** has an amplitude of 0.154 in fractional coordinates. A small

* The interlayer shift vectors describe the shortest translation in the **a-b** plane required to stack all the Si and Al atoms of the interlayer sheets over one another. The vectors are defined either in fractional coordinates of a 2-D hexagonal unit cell (describing symmetry of individual Al and Si sheets) with a_h=5.1 Å, or in fractional coordinates of a 2-D rectangular unit cell with a_r = 5.1 Å, b_r = 8.9 Å, as distinguished by a subscript h or r following the coordinates.

† This class includes the following six vectors: $[-2/3, -1/3]_h$, $[1/3, 2/3]_h$, $[-1/3, 1/3]_h$, $[1/3, -1/3]_h$, $[2/3, 1/3]_h$, and $[-1/3, -2/3]_h$.

‡ This class includes the following six vectors: $[1/3, 0]_h$, $[0, -1/3]_h$, $[-1/3, -1/3]_h$, $[-1/3, 0]_h$, $[0, 1/3]_h$, and $[1/3, 1/3]_h$.

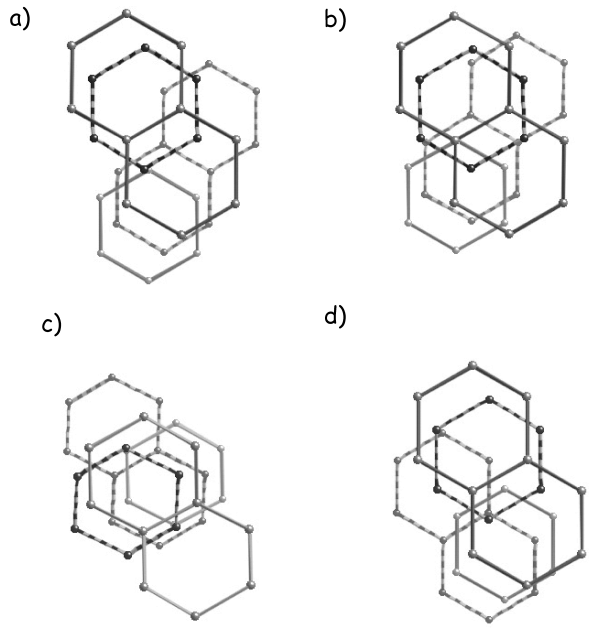

FIGURE 1. Overlapping of neighboring 1:1 layers in different kaolin polytypes (**a**) dickite; (**b**) high-pressure dickite; (**c**) kaolinite; and (**d**) nacrite. The structures in the left column exhibit Type I connections, those in the right column represent Type II connections. All projections are shown approximately normal to the layers, with the **b** axis vertical, except for nacrite, for which the **a** axis is vertical. The O and H atoms are omitted for clarity. The lines connect Si (dashed) and Al ions (solid). The light gray lines correspond to the lower layer, dark gray ones to the upper layer.

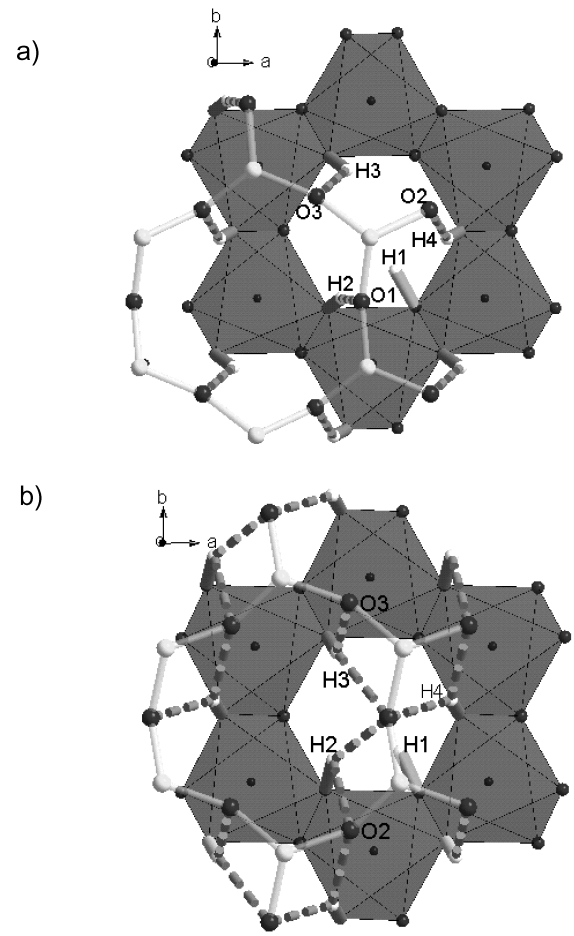

FIGURE 2. Interlayer connections in low- and high-pressure dickite. The polyhedra represent Al coordination spheres, and dashed lines correspond to hydrogen bonds. The apical O atoms of the Si sheet have been removed for clarity. The rings are formed by Si and Al ions. The hydrogen atoms are omitted for clarity. The donor and acceptor O atoms involved in the same hydrogen bond are connected by solid lines.

change in the z-coordinate, by 0.005 on average, results from the ~7° change in β angle. An additional shift along **a** by $[0.160, 0]_r$ results from the change in β angle as well. In effect, the resulting final average layer shift vector is $[0.146, 0.154]_r$, which agrees well with the predicted shift of $[1/6, 1/6]_r$. As mentioned above, layer stacking in high-pressure dickite is Type II, as in nacrite. The structure of high-pressure dickite, however, is different from that of nacrite because of the different rotational relation between neighboring layers. The distinction between different Si tetrahedra in high-pressure dickite is diminished, and both types of tetrahedra are placed approximately equidistantly from two octahedra in the Al layer. The hydrogen bonds from the corners of these tetrahedra are linked to three O atoms in two neighboring octahedra, as illustrated in Figure 2.

In the description introduced by Zvyagin (1962), the translational and rotational relations between the neighboring pseudohexagonal sheets of atoms in the structure of a clay mineral are described by means of intralayer shift vectors (σ) and interlayer shift vectors (τ). The σ shifts were defined as the shortest translation in the **a-b** plane necessary to bring all the Si and Al atoms of the same 1:1 layer to overlap over each other, whereas τ is the shortest translation required to bring to overlap the nearest Si and Al atoms belonging to two neighboring 1:1 layers. For a structure with two-layer periodicity, five symbols are required to fully describe the stacking sequence. The allowed translation amplitudes are 1.7 Å for translation by $a_o/3$, 3.0 Å for translation by $b_o/3$, and 3.4 Å for translation by $a_o/3 + b_o/3$. The last translation vector, $a_o/3 + b_o/3$, can be alternatively represented in the hexagonal translations as $2b_h/3$ or $-b_h/3$ (amplitude 1.7 Å in the direction opposite to $a_o/3 + b_o/3$). It is worth noting that all the σ translations have the same amplitude (1.7 Å, or 5.1 Å – 3.4 Å = 1.7 Å), whereas there are two classes of τ translations, corresponding to the stacking types τ_+ and τ_-, with amplitudes 3.0 Å (Type I), and τ_1, τ_2, τ_3, τ_4, τ_5, and τ_6, with amplitudes 1.7 Å (Type II). In Zvyagin's notation dickite is represented by $\sigma_1\tau_+\sigma_5\tau_-\sigma_1$ (structure I4 in Table 4; Zvyagin 1962), kaolinite as $\sigma_2\tau_+\sigma_2\tau_+\sigma_2$ (structure I1/I2) or, in abbreviated version, $\sigma_2\tau_+\sigma_2$, and nacrite as $\sigma_1\tau_2\sigma_2\tau_1\sigma_1$ (structure III1). The meaning of the subscripts is explained in Table 1 of Zvyagin (1962). Layer shift transformations found in dickite leave the intralayer translations (and relative layer rotations) unchanged. Therefore the symbol of a new structure will have the same σ components, whereas the τ components will change type. Following these rules high-pressure dickite will be represented by $\sigma_1\tau_3\sigma_5\tau_3\sigma_1$, described as structure IV4.

The fact that a shift of layers may lead to another energetically stable stacking configuration was recognized as early as in 1938 (Hendricks 1940; Hendricks and Jefferson 1938). The concept was then extensively applied to develop models describing stacking disorder in kaolin minerals (see Giese 1991 for review). However, the idea that the interlayer shift may be utilized to produce a different, ordered polytype phase has not been widely accepted [an exception is the work by DeLuca and Slaughter (1985), who suggested the existence of multiple differently ordered phases of kaolinite, related to each other by layer shift along **b**]. Based on our results we conclude that the layer shift is indeed a basis for the existence of previously unknown, ordered kaolin polytypes that may be stable at high pressure.

The mechanism of low-to-high-pressure transformation in dickite

Si^{4+} and Al^{3+} ions within neighboring sheets directly overlap each other in dickite. One of the arguments as to why the layer shift produced by the pressure-induced transition is favored may be a tendency to minimize the electrostatic interlayer repulsion. Giese (1973) performed simple interlayer electrostatic interaction estimations that showed that the repulsion is stronger for kaolinite than for nacrite; however, the value obtained for dickite, most likely due to the crudeness of the approximation, was closer to that of nacrite than to kaolinite. The direction perpendicular to the layers is the most compressible in the dickite structure, and compression of hydrogen bonds in the interlayer region increases as pressure increases (and *c* decreases), as does the electrostatic interlayer repulsion. The phase transition changes the geometry of the hydrogen bonding in the interlayer and provides an opportunity for hydroxyl groups to assume a more relaxed configuration by changing proton acceptors after the layer shift.

The transformation is displacive and fully reversible, which means that the high-pressure form is not thermodynamically stable at low pressure. The reversibility of the transition is interesting, considering that nacrite, which exhibits the same layer stacking type as high-pressure dickite, occurs in nature under ambient conditions. This fact is most likely a consequence of a subtle balance between the interlayer cohesion forces that are influenced by longer-range interactions resulting from different rotational relations between neighboring layers. On the other hand, from an electrostatic repulsion perspective, the occurrence of Type-II interlayer connections in nacrite, which should be less energetically favorable than Type-I connections, is in agreement with the observations made by DeLigny and Navrotsky (1999) that nacrite is the least stable among the kaolin minerals and may in fact be a metastable phase.

Hydrostatic compressibility

The pressure dependence of unit-cell parameters is illustrated in Figure 3, and the values of unit-cell parameters at different pressures are given in Table 3. Because of the availability of two pressure points for each phase of dickite, only estimates of linear compressibility were calculated and are presented in Table 4. Although these results give some semiquantitative description of the elastic properties of both phases, the small number of sampling points most likely cause a significant overestimation of the bulk moduli (see Wang et al. 1980 for a comparison). The phase transition is accompanied by a decrease in the unit-cell volume of about 2% and a 7° reduction in the β angle. The intralayer compressibility in the high-pressure phase remains similar to that of the low-pressure phase, whereas the compressibility along the direction normal to the layers decreases as a consequence of a shorter layer-layer distance in the interlayer and increased interlayer interactions. As a result, the high-pressure phase is stiffer and has a higher bulk modulus.

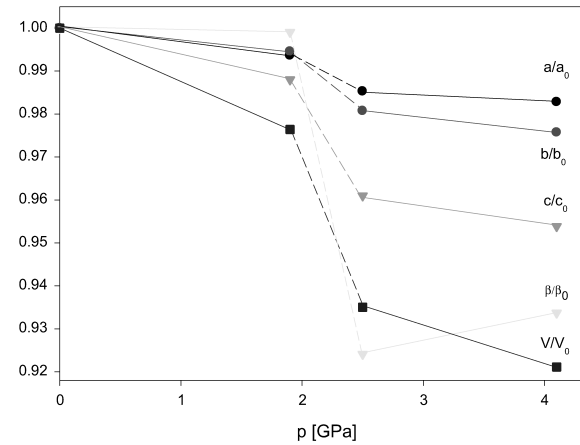

FIGURE 3. Hydrostatic compressibility of dickite, showing the isosymmetric displacive layer-shift phase transition between 1.9 and 2.5 GPa.

TABLE 3. Pressure dependence of lattice parameters

P (GPa)	*a* (Å)	*b* (Å)	*c* (Å)	β (°)	*V* (Å³)
1e-4	5.161(3)	8.960(6)	14.46(1)	96.77(1)	663.9(7)
1.9	5.138(3)	8.926(5)	14.26(1)	96.73(2)	649.7(6)
2.5	5.095(3)	8.802(6)	13.874(9)	89.47(2)	622.2(7)
4.1	5.082(3)	8.757(6)	13.77(1)	89.60(2)	612.9(7)

TABLE 4. Estimates of linear compressibility and bulk modulus (calculated as an inverse of compressibility coefficient) for low- and high- pressure dickite

	β_a (10^{-3} GPa)	β_b (10^{-3} GPa)	β_c (10^{-3} GPa)	B_0 (GPa)
Low-P dickite	2.3	2.0	7.1	88.8
High-P dickite	1.6	3.2	4.6	107.6

Note: The parameters for each phase are calculated based on only two available data points.

The geometry of coordination polyhedra

The changes in primary bond lengths from 0.1 MPa to 4.1 GPa are not very pronounced. The Al-O bonds were affected by pressure much more than the Si-O bonds, with an average shortening by about 0.9% of the former and by about 0.1% of the latter. The bond angles in the polyhedra were also affected only slightly. The O-Al-O angles involving two O atoms shared between two neighboring AlO_6 octahedra (edge sharing) are significantly smaller than the other octahedral O-Al-O angles. As a result of the pressure-induced transformation, the mean value of this class of O-Al-O angles increased by ~1° on average. Also, the octahedral O-Al-O angles between two opposite

TABLE 5. The results of simulated annealing and energy minimization based determination of hydrogen atom positions in low- and high-pressure dickite

Atom	Low-pressure dickite			High-pressure dickite					
	x	*y*	*z*	*x*	*y*	*z*	Δx	Δy	Δy
Si1	0.0091	0.4012	0.0321	0.0503	0.4882	0.0286	0.0412	0.0870	–0.0035
Si2	–0.0032	0.0723	0.0315	0.0348	0.1587	0.0304	0.0380	0.0864	–0.0011
Al1	0.9123	0.2525	0.2230	0.8786	0.3308	0.2359	–0.0337	0.0783	0.0129
Al2	0.4190	0.4173	0.2224	0.3954	0.4997	0.2397	–0.0236	0.0824	0.0173
O1	0.9570	0.2394	0.9864	0.9832	0.3195	0.9862	0.0262	0.0801	–0.0002
O2	0.2552	0.4715	0.9854	0.3221	0.5444	–0.0069	0.0669	0.0729	0.0077
O3	0.7639	0.5057	0.9992	0.8191	0.6005	0.0029	0.0552	0.0948	0.0037
O4	0.0789	0.3903	0.1433	0.0754	0.4784	0.1428	–0.0035	0.0881	–0.0005
O5	0.0028	0.0808	0.1441	0.0058	0.1683	0.1458	0.0030	0.0875	0.0017
OH1	0.5827	0.2734	0.1488	0.5743	0.3532	0.1382	–0.0084	0.0798	–0.0106
OH2	0.2433	0.2772	0.2873	0.1971	0.3513	0.3016	–0.0462	0.0741	0.0143
OH3	0.2493	0.8939	0.2897	0.2056	0.9784	0.2945	–0.0437	0.0845	0.0048
OH4	0.3236	0.5840	0.2874	0.2600	0.6662	0.3054	–0.0636	0.0822	0.0180
H1	0.4993	0.1830	0.1625	0.4964	0.2556	0.1421	–0.0029	0.0726	–0.0204
H2	0.3222	0.2524	0.3469	0.2349	0.2821	0.3511	–0.0873	0.0297	0.0042
H3	0.3450	0.9270	0.3454	0.2518	0.0170	0.3557	–0.0932	–0.9100	0.0103
H4	0.2893	0.6009	0.3504	0.2329	0.6346	0.3701	–0.0564	0.0337	0.0197

Note: The average shifts of atoms in high-pressure dickite, relative to dickite, expressed in fractional atomic coordinates are $\Delta x = -0.014$, $\Delta y = 0.077$, $\Delta z = 0.005$. The estimated standard deviations are omitted because the method of calculation, based on energy minimization, does not allow for their determination.

apices straightened, becoming closer to 180° by about 2.5°. The tetrahedral O-Si-O bond angles were almost unaffected. As a result of the change in interlayer bonding accompanying the phase transition, the distance between the centers of the nearest pseudo-hexagonal rings formed by Al and Si ions of the neighboring layers decreased dramatically from 5.414 to 4.515 Å (nearly 17%), whereas the unit cell was compressed perpendicular to the layers by only about 8%.

Hydroxyl group orientations

The issue of determining orientations of hydroxyl groups in clay minerals is very important because of the crucial role hydrogen bonds play among the interlayer cohesion forces. Unfortunately, at the same time, it represents a great experimental challenge because of the low quality of single-crystal specimens and insufficient sensitivity of X-ray diffraction methods to hydrogen atoms. We anticipated on the basis of the Raman high-pressure results that the observed phase transition involves significant changes in the hydrogen atom positions and environment. Furthermore, on the basis of the structure model of high-pressure dickite, it is obvious that the transformation requires breaking and re-formation of interlayer hydrogen bonds. However, a detailed understanding of the mechanism of this transformation requires knowledge of the atomic positions of hydrogen atoms above and below the transition. To circumvent the difficulty of locating hydrogen atoms in the dickite structure using X-ray data, we applied an approach based on a combination of simulated annealing and energy minimization (SA&EM), as implemented in the Endeavour program (Putz et al. 1999; Crystal Impact 2001). We first optimized the refined models of both low- and high-pressure dickite containing only non-hydrogen atoms. The cost function, determining significance of the contribution of each of these search methods, was set at an X-ray data contribution of 80%. After this initial optimization, the positions of four symmetry-independent hydrogen atoms were determined by the same method, with the non-hydrogen atoms fixed. The last step was a local optimization (refinement) of the positions of all the atoms in the structure. The SA&EM methodology was tested by determining hydrogen-atom positions for the ambient-pressure dickite. The results obtained were in good agreement with published data. There has been considerable ambiguity in the literature concerning the orientation of the inner-OH group in dickite. Giese and Datta (1973) calculated the orientations of OH groups using electrostatic potentials. Adams and Hewat (1981) used neutron powder diffraction, and Rozhdestvenkaya et al. (1982), SenGupta et al. (1984), and Joswig and Drits (1986) used single-crystal X-ray diffraction to determine the positions of the hydrogen atoms. Recently, Bish and Johnston (1993) used neutron powder diffraction and infrared spectroscopy to locate more accurately the hydrogen atoms in dickite. In addition, analysis of the local Raman tensor obtained from a single-crystal Raman study of an oriented dickite crystal provided complementary structural information about the orientations of the OH groups (Johnston et al. 1998). Recently, Benco et al. (2001a,b) performed ab initio molecular dynamics simulations to explain the previous findings. All the positions of intra-layer hydroxyl groups in our case agree well with the previous studies. The orientation of the inner hydroxyl group we determined is, however, closer to the results of Rozhdestvenkaya et al. (1982) and Benco et al. (2001a,b), showing an inclination angle to the (001) plane of about 12°, as opposed to the conclusions of Joswig and Drits (1986) and Bish and Johnston (1993), which showed an inclination of ~1° from the (001) plane. The fractional atomic coordinates of all atoms obtained from the Monte-Carlo optimization are presented in Table 5. The parameters describing the geometry of hydrogen bonds are presented in Table 6. Similarly, as suggested by Joswig and Drits (1986), Bish and Johnston (1993), and Benco et al. (2001b), we found that two of the interlayer OH groups (OH2 and OH4) participate in relatively strong hydrogen bonds, with proton-acceptor distances of about 2 Å and donor-proton-acceptor (D-H···A) angles close to 160°. The third interlayer OH group forms a much weaker hydrogen bond, with a D···A distance of almost 3.152 Å and a D-H···A angle of 138.1°.

Having confirmed that our method could be used success-

TABLE 6. The geometry of interlayer O-H···O contacts in low- and high-pressure dickite, based on atomic coordinates determined by SA&EM

D	H	A	Next A (A')	D-H	H···A	D···A	D-H···A	H···A'	D···A'	D-H···A'
Low-P dickite at 0.1 MPa										
OH2	H2	O1		0.935	2.005	2.962	162.8			
OH3	H3	O3		0.941	2.388	3.152	138.1			
OH4	H4	O2		0.960	2.084	2.967	152.2			
High-P dickite at 4.1 GPa										
OH2	H2	O1	O2	0.931	2.411	3.281	155.4	2.513	2.858	102.2
OH3	H3	O3	O1	0.937	2.296	3.004	131.9	2.576	3.470	159.9
OH4	H4	O2	O1	0.945	2.350	3.190	147.9	2.087	2.872	139.5

Notes: The distances are given in angstroms and the angles in degrees. The estimated standard deviations are omitted because the method of calculation of H positions, based on energy minimization, does not allow for their determination.

fully for determination of hydrogen atom positions at ambient pressure, we applied the same approach to high-pressure dickite. Our attempt yielded hydrogen atom positions for the high-pressure phase in good agreement with the topological model of the phase transition mechanism and change in the interlayer connection scheme presented above. As a result of the fact that in high-pressure dickite every Si^{4+} ion becomes approximately equidistant from two adjacent Al^{3+} ions, there are more than three symmetry-independent close H···O contacts. Every interlayer H atom is involved in close contacts with two, instead of one, O atom, as shown in Table 6. This fact affects the orientations of hydroxyl groups that are directed more between the two nearest O atoms than toward any one of them. As a result of the bifurcated nature of hydrogen bonds in high-pressure dickite, all the D-H···A angles for hydrogen bonds present in low-pressure dickite are reduced, and bonding distances elongated. For H3 alone, the new contact to O1 is relatively distant (D···A of 3.47 Å) and thus it has the smallest effect on the original bond. The inner hydroxyl group remains almost unaffected (the inclination angle decreases to 6°), whereas the interlayer OH groups change their orientation to form new hydrogen bonds.

The fact that the number of interlayer hydrogen bonds in high-pressure dickite is doubled, as compared with dickite, means that the contribution of the hydrogen bonds to the overall compressibility along this direction should be more significant (despite the fact that the average H-O distance is longer than in dickite). This conclusion is in agreement with our observation of decreased compressibility along the **c** direction in high-pressure dickite.

These results clarify the mechanism of the pressure-induced phase transition and also show the resilience of individual 1:1 layers. Considering the similarities in the structures of kaolin polytypes and the simple mechanism of this transformation in dickite, it is tempting to predict whether similar transformations will occur for the other polytypes. For kaolinite, one may expect ion overlapping to become similarly unfavorable at high pressure. A hypothetical high-pressure form of kaolinite, created by a shift of layers similar to that observed in dickite, should result in a doubling along the **c** direction, as compared with kaolinite. Indirect evidence for the occurrence of multiple phases of kaolinite resulting from grinding (nonhydrostatic compression) was presented by DeLuca and Slaughter (1985). Remarkably, these authors proposed a model for a hypothetical new variety of kaolinite that involved a shift of layers along **b** by a vector of an arbitrary length. The nacrite structure has interlayer connections of Type II under ambient pressure. Of course, one can imagine a transformation to Type-I stacking, but if we accept the assumption that ion overlapping in Type I becomes energetically unfavorable at high pressure, it would be surprising if such an inverse transformation occurs. On the other hand, if we accept the suggestion of DeLigny and Navrotsky (1999) that nacrite is not thermodynamically stable under ambient conditions, but rather is metastable, then a change in thermodynamic conditions (not necessarily just pressure) may induce a transformation to a more stable and quenchable Type-I structure.

A potential important geological consequence of the observation presented in this study is the increase of the elastic modulus of dickite (and of kaolinite if we assume generality of the low- to high-pressure transformation) in the high-pressure phase. If kaolin minerals occur at depths corresponding to pressures up to 3.5 GPa there should be a discontinuity in the elastic properties corresponding to the low- to high-pressure transformation of kaolin minerals.

The presented mechanism of layer-shift phase transition does not provide a method of interconversion between the polytypes that differ by rotation of 1:1 layers. Transformations like this have been suggested to occur as a function of depth (pressure) in sandstone reservoirs (Beaufort 1998; Ehrenberg et al. 1993). From our observations it seems that such transformations must occur through dissolution or reconstructive solid-solid mechanisms rather than through a displacive mechanism.

The role of temperature in driving layer-shift phase transition was not examined in our experiments, as all were performed at ambient temperature. However, temperature may be a very important factor as a multitude of local energy minima with almost equal depths, which are separated from each other by relatively high energy barriers, may easily result in formation of metastable phases. Therefore, further systematic high-*PT* studies would be very important.

The results presented in this study were stimulated by the Raman experiments of Johnston et al. (2002) and provide good explanation of the changes observed in Raman spectra above 2 GPa. Our results also constitute the first complete high-pressure structural evaluation of a kaolin mineral and the first determination of hydrogen atom positions from a combination of laboratory in situ high-pressure data and theoretical modeling. We hope that the combination method we applied here will find more future applications in high-pressure crystallography.

ACKNOWLEDGMENTS

This study was primarily supported by funding from NSF grant EAR9973018 and by LDRD funding at the Los Alamos National Laboratory. We thank H. Yang for help with sample preparation.

REFERENCES CITED

Adams, J.M. and Hewat, A.W. (1981) Hydrogen atom positions in dickite. Clays and Clay Minerals, 29, 316–319.

Altomare, A., Burla, M.C., Camalli, M., Cascarano, G.L., Giacovazzo, C., Guagliardi, A., Moliterno, A.G.G., Polidoro, G. and Spagna, R. (1996). SIR97. A Program for the Automatic Solution and Refinement of Crystal Structures. University of Bari, Italy.

Beaufort, D. (1998) Kaolinite-to-dickite reaction in sandstone reservoirs. Clay Minerals, 33, 297.

Benco, L., Tunega, D., Hafner, J., and Lischka, H. (2001a) Ab-initio density functional theory applied to the structure and proton dynamics of clays. Chemical Physics Letters, 333, 479–484.

——— (2001b) Orientation of OH groups in kaolinite and dickite: Ab initio molecular dynamics study. American Mineralogist, 86, 1057–1065.

Bish, D.L. and Johnston, C.T. (1993) Rietveld refinement and Fourier-transform infrared spectroscopic study of the dickite structure at low temperature. Clays and Clay Minerals, 41, 297–304.

Brindley, G.W. and Brown, G. (1980) Crystal Structures of clay minerals and their X-ray identification. Mineralogical Society, London.

Catti, M., Ferraris, G., Hull, S., and Pavese, A. (1994) Powder neutron diffraction study of 2M1 muscovite at room pressure and at 2 GPa. European Journal of Mineralogy, 6, 171–178.

Catti, M., Ferraris, G., Hull, S., and Pavese, A. (1995) Static compression and H disorder in brucite, $Mg(OH)_2$, to 11 GPa: a powder neutron diffraction study. Physical Chemistry of Minerals, 22, 200–206.

Christy, A.G. (1993) Multistage diffusionless pathways for reconstructive phase transitions: application to binary compounds and calcium carbonate. Acta Crystallographica, B49, 987–996.

——— (1995) Isosymmetric structural phase transitions: Phenomenology and examples. Acta Crystallographica, B51, 753–757.

Comodi, P. and Zanazzi, P.F. (1995) High pressure structural study of muscovite. Physics and Chemistry of Minerals, 22, 170–177.

——— (1997) Pressure dependence of structural parameters of paragonite. Physics and Chemistry of Minerals, 24, 174–180.

Crystal Impact (2001) G. Endeavour 1.1, Internet: http://www.crystalimpact.com/endeavour, Email: info@crystalimpact.com. Endeavour, Bonn.

DeLigny, D. and Navrotsky, A. (1999) Energetics of kaolin polymorphs. American Mineralogist, 84, 506–516.

DeLuca, S. and Slaughter, M. (1985) Existence of multiple kaolinite phases and their relationship to disorder in kaolin minerals. American Mineralogist, 70, 149–158.

Dove, M.T., Trachenko, K.O., Tucker, M.G., and Keen, D.A. (2000) Rigid Unit Modes in framework structures: theory, experiment and applications. In S.A.T. Redfern and M.A. Carpenter, Eds., Transformation processes in minerals, 39, p. 1–33. Reviews in Mineralogy, Mineralogical Society of America, Washington, D.C.

Duffy, T.S., Meade, C., Fei, Y., Mao, H.-K., and Hemley, R.J. (1995) High-pressure phase transition in brucite, $Mg(OH)_2$. American Mineralogist, 80, 222–230.

Ehrenberg, S.N., Aagaard, P., Wilson, M.J., Fraser, A.R., and Duthie, D.M.L. (1993) Depth-dependent transformation of kaolinite to dickite in sandstones of the Norwegian continental shelf. Clay Minerals, 28, 325–352.

Faust, J. and Knittle, E. (1994) The equation of state, amorphisation and high pressure phase diagram of muscovite. Journal of Geophysical Research, 99, 19785–19792.

Giese, R.F. (1973) Interlayer bonding in kaolinite, dickite and nacrite. Clays and Clay Minerals, 21, 145–149.

——— (1991) Kaolin minerals: Structures and stabilities. In S.W. Bailey, Ed., Hydrous phyllosilicates, 19, 29–66. Reviews in Mineralogy, Mineralogical Society of America, Washington, D.C.

Giese, R.F.J. and Datta, P. (1973) Hydroxyl orientation in kaolinite, dickite, and nacrite. American Mineralogist, 58, 471–479.

Hazen, R.M. and Finger, L.W. (1978) The crystal structures and compressibilities of layer minerals at high pressure. II. Phlogopite and chlorite. American Mineralogist, 63, 293–296.

Hendricks, S.B. (1940) Variable structures and continuous scattering of X-rays from layer silicate lattices. Physical Review, 57, 448–454.

Hendricks, S.B. and Jefferson, M.E. (1938) Structures of kaolin and talc-pyrophyllite hydrates and their bearing on water sorption of the clays. American Mineralogist, 23, 863–875.

Holtz, M., Solin, S.A., and Pinnavaia, T.J. (1993) Effect of pressure on the Raman vibrational modes of layered aluminosilicate compounds. Physical Review B, 48, 13312–13317.

Huang, E., Li, A., Xu, J., Chen, R., and Yamanaka, T. (1996) High-pressure phase transition in $Al(OH)_3$: Raman and X-ray observations. Geophysical Research Letters, 23, 3083–3086.

Huang, E., Lin, J.-F., Xu, J., Huang, T., Jean, Y.-C., and Sheu, H.-S. (1999) Compression studies of gibbsite and its high pressure polymorph. Physics and Chemistry of Minerals, 26, 576–583.

Johnston, C.T., Wang, S.L., Bish, D.L., Dera, P., Agnew, S.F., and Kenney, J.W.II (2002) Novel pressure induced phase transformations in hydrous layered materials: a comparative single crystal high pressure Raman/XRD study of dickite and gibbsite. Geophysical Research Letters, 29, 1029.

Joswig, W. and Drits, V.A. (1986) The orientation of the hydroxyl groups in dickite by X-ray diffraction. Neues Jahrbuch für Mineralogie Monatshefte, 1, 19–22.

LaIglesia, A. (1993) Pressure induced disorder in kaolinite. Clay Minerals, 28, 311–319.

Murray, H.H. (1991) Kaolin minerals: Their genesis and occurances. In S.W. Bailey, Ed., Hydrous phyllosilicates, 19, 29–66. Reviews in Mineralogy, Mineralogical Society of America, Washington, D.C.

Newnham, R.E. (1961) A refinement of the dickite structure and some remarks on polytypism in kaolin minerals. Mineralogical Magazine, 32, 683–703.

Parise, J.B., Leinenweber, K., Weidner, D.J., Tan, K., and Dreele, R.B.V. (1994) Pressure-induced H bonding: Neutron diffraction study of brucite, $Mg(OD)_2$, to 9.3 GPa. American Mineralogist, 79, 193–196.

Putz, H., Schon, J.C., and Jansen, M. (1999) Combined method for 'Ab initio' structure solution from powder diffraction data. Journal of Applied Crystallography, 32, 864–870.

Rozhdestvenkaya, I.V., Bookin, A.S., Drits, V.A., and Finko, V.I. (1982) Proton positions and structural characteristics of dickite by X-ray diffraction. Mineral Zhurnal, 4, 52–58.

SenGupta, P.K., Schlemper, E.O., Johns, W.D., and Ross, F. (1984) Hydrogen positions in dickite. Clays and Clay Minerals, 32, 483–485.

Sheldrick, G.M. (1997). SHELXL97. Program for the Refinement of Crystal Structures. University of Gottingen, Germany.

Velde, B. (1969) The compositional join muscovite-pyrophyllite at moderate temperature and pressure. Bulletin de la Societe Francaise Mineralogie et de Cristallographie, 92, 360.

Verma, A.R. and Krishna, P. (1966) Polymorphism and polytypism in crystals. Wiley, New York.

Wang, C.-Y., Lin, W., and Wu, F.T. (1978) Constitution of the San Andreas fault zone at depth. Geophysical Research Letters, 5, 741.

Wang, C.-Y., Mao, N.-H., and Wu, F.T. (1979) The mechanical property of montmorillonite clay at high pressure and implications on fault behavior. Geophysical Research Letters, 6, 476–478.

———(1980) Mechanical properties of clays at high pressure. Journal of Geophysical Research, 85, 1462–1468.

Zoback, M.D. and Roller, J.C. (1979) Magnitude of shear stress on the San Andreas fault: implications of a stress measurment profile at shallow depth. Science, 206, 445.

Zvyagin, B.B. (1962) Polymorphism of double-layer materials of the kaolinite type. Soviet Physics, Crystallography, 7, 38–51.

MANUSCRIPT RECEIVED AUGUST 23, 2002
MANUSCRIPT ACCEPTED APRIL 13, 2003
MANUSCRIPT HANDLED BY GEORGE LAGER